Fiber-optic Cherenkov radiation in the few-cycle regime

Guoqing Chang,* Li-Jin Chen, and Franz X. Kärtner

Department of Electrical Engineering and Computer Science and Research Laboratory of Electronics, Massachusetts Institute of Technology, 77 Massachusetts Avenue, Cambridge, Massachusetts 02139, USA
**guoqing@mit.edu*

Abstract: Fiber-optic Cherenkov radiation has emerged as a wavelength conversion technique to achieve isolated spectrum in the visible wavelength range. Most published results have reinforced the impression that CR forms a narrowband spectrum with poor efficiency. We both theoretically and experimentally investigate fiber-optic Cherenkov radiation excited by few-cycle pulses. We introduce the *coherence length* to quantify the Cherenkov-radiation bandwidth and its dependence on propagation distance. Detailed numerical simulations verified by experimental results reveal three unique features that are absent when pumped with often-used, long pulses; that is, continuum generation (may span one octave in connection with the pump spectrum), high conversion efficiency (up to 40%), and broad bandwidth (70 nm experimentally obtained) for the isolated Cherenkov radiation spectrum. These merits allow achieving broadband visible-wavelength spectra from low-energy ultrafast sources which opens up new applications (e.g. precision calibration of astronomical spectrographs).

OCIS codes: (140.3510) Lasers, fiber; (190.7110) Ultrafast nonlinear optics; (060.4370) Nonlinear optics, fibers.

References and links

1. P. K. A. Wai, C. R. Menyuk, Y. C. Lee, and H. H. Chen, "Nonlinear pulse propagation in the neighborhood of the zero-dispersion wavelength of monomode optical fibers," Opt. Lett. **11**(7), 464–466 (1986).
2. P. K. A. Wai, H. H. Chen, and Y. C. Lee, "Radiations by "solitons" at the zero group-dispersion wavelength of single-mode optical fibers," Phys. Rev. A **41**(1), 426–439 (1990).
3. V. I. Karpman, "Radiation by solitons due to higher-order dispersion," Phys. Rev. E Stat. Phys. Plasmas Fluids Relat. Interdiscip. Topics **47**(3), 2073–2082 (1993).
4. N. Akhmediev and M. Karlsson, "Cherenkov radiation emitted by solitons in optical fibers," Phys. Rev. A **51**(3), 2602–2607 (1995).
5. J. N. Elgin, T. Brabec, and S. M. J. Kelly, "A perturbative theory of soliton propagation in the presence of third order dispersion," Opt. Commun. **114**(3–4), 321–328 (1995).
6. K. Saitoh, M. Koshiba, T. Hasegawa, and E. Sasaoka, "Chromatic dispersion control in photonic crystal fibers: application to ultra-flattened dispersion," Opt. Express **11**(8), 843–852 (2003).
7. D. V. Skryabin, F. Luan, J. C. Knight, and P. St. J. Russell, "Soliton self-frequency shift cancellation in photonic crystal fibers," Science **301**(5640), 1705–1708 (2003).
8. S. Stark, F. Biancalana, A. Podlipensky, and P. St. J.Russell, "Nonlinear wavelength conversion in photonic crystal fibers with three zero dispersion points," Phys. Rev. A **83**(2), 023808 (2011).
9. D. V. Skryabin and A. V. Yulin, "Theory of generation of new frequencies by mixing of solitons and dispersive waves in optical fibers," Phys. Rev. E Stat. Nonlin. Soft Matter Phys. **72**(1), 016619 (2005).
10. A. V. Husakou and J. Herrmann, "Supercontinuum generation of higher-order solitons by fission in photonic crystal fibers," Phys. Rev. Lett. **87**(20), 203901 (2001).
11. A. V. Husakou and J. Herrmann, "Supercontinuum generation, four-wave mixing, and fission of higher- order solitons in photonic-crystal fibers," J. Opt. Soc. Am. B **19**(9), 2171–2182 (2002).
12. L. Tartara, I. Cristiani, and V. Degiorgio, "Blue light and infrared continuum generation by soliton fission in a microstructured fiber," Appl. Phys. B **77**(2–3), 307–311 (2003).
13. G. Genty, M. Lehtonen, and H. Ludvigsen, "Effect of cross-phase modulation on supercontinuum generation in microstructured fibers with sub-30 fs pulses," Opt. Express **12**(19), 4614–4624 (2004).
14. D. R. Austin, C. M. de Sterke, B. J. Eggleton, and T. G. Brown, "Dispersive wave blue-shift in supercontinuum generation," Opt. Express **14**(25), 11997–12007 (2006).

#140545 - $15.00 USD Received 4 Jan 2011; revised 22 Feb 2011; accepted 10 Mar 2011; published 23 Mar 2011

15. A. V. Gorbach and D. V. Skryabin, "Light trapping in gravity-like potentials and expansion of supercontinuum spectra in photonic-crystal fibres," Nat. Photonics **1**(11), 653–657 (2007).
16. S. P. Stark, A. Podlipensky, N. Y. Joly, and P. St. J. Russell, "Ultraviolet-enhanced supercontinuum generation in tapered photonic crystal fiber," J. Opt. Soc. Am. B **27**(3), 592–598 (2010).
17. J. M. Dudley, G. Genty, and S. Coen, "Supercontinuum generation in photonic crystal fiber," Rev. Mod. Phys. **78**(4), 1135–1184 (2006).
18. S. Roy, S. K. Bhadra, and G. P. Agrawal, "Effects of higher-order dispersion on resonant dispersive waves emitted by solitons," Opt. Lett. **34**(13), 2072–2074 (2009).
19. A. A. Amorim, H. M. Crespo, M. Miranda, J. L. Silva, and L. M. Bernardo, "Study of non-solitonic blue-green radiation generated in mm-long photonic crystal fibers," Proc. SPIE **6187**, 618717 (2006).
20. A. V. Mitrofanov, Y. M. Linik, R. Buczynski, D. Pysz, D. Lorenc, I. Bugar, A. A. Ivanov, M. V. Alfimov, A. B. Fedotov, and A. M. Zheltikov, "Highly birefringent silicate glass photonic-crystal fiber with polarization-controlled frequency-shifted output: A promising fiber light source for nonlinear Raman microspectroscopy," Opt. Express **14**(22), 10645–10651 (2006).
21. H. Tu and S. A. Boppart, "Optical frequency up-conversion by supercontinuum-free widely-tunable fiber-optic Cherenkov radiation," Opt. Express **17**(12), 9858–9872 (2009).
22. H. Tu and S. A. Boppart, "Ultraviolet-visible non-supercontinuum ultrafast source enabled by switching single silicon strand-like photonic crystal fibers," Opt. Express **17**(20), 17983–17988 (2009).
23. G. Q. Chang, L.-J. Chen, and F. X. Kärtner, "Highly efficient Cherenkov radiation in photonic crystal fibers for broadband visible wavelength generation," Opt. Lett. **35**(14), 2361–2363 (2010).
24. F. X. Kärtner, ed., *Few-Cycle Laser Pulse Generation and Its Applications* (Springer, 2004).
25. S. Hill, C. E. Kuklewicz, U. Leonhardt, and F. König, "Evolution of light trapped by a soliton in a microstructured fiber," Opt. Express **17**(16), 13588–13600 (2009).
26. G. Krauss, S. Lohss, T. Hanke, A. Sell, S. Eggert, R. Huber, and A. Leitenstorfer, "Synthesis of a single cycle of light with compact erbium-doped fibre technology," Nat. Photonics **4**(1), 33–36 (2010).
27. G. P. Agrawal, *Nonlinear Fiber Optics*, 3rd ed. (Academic Press, 2001).
28. Q. Lin and G. P. Agrawal, "Raman response function for silica fibers," Opt. Lett. **31**(21), 3086–3088 (2006).
29. A. Nahata, A. S. Weling, and T. F. Heinz, "A wideband coherent terahertz spectroscopy system using optical rectification and electro-optic sampling," Appl. Phys. Lett. **69**(16), 2321–2323 (1996).
30. Y. Kodama and A. Hasegawa, "Nonlinear pulse propagation in a monomode dielectric guide," IEEE J. Quantum Electron. **23**(5), 510–524 (1987).
31. S. Roy, S. K. Bhadra, and G. P. Agrawal, "Effects of higher-order dispersion on resonant dispersive waves emitted by solitons," Opt. Lett. **34**(13), 2072–2074 (2009).
32. M. T. Murphy, T. Udem, R. Holzwarth, A. Sizmann, L. Pasquini, C. Araujo-Hauck, H. Dekker, S. D'Odorico, M. Fischer, T. W. Hänsch, and A. Manescau, "High-precision wavelength calibration of astronomical spectrographs with laser frequency combs," Mon. Not. R. Astron. Soc. **380**(2), 839–847 (2007).
33. C.-H. Li, A. J. Benedick, P. Fendel, A. G. Glenday, F. X. Kärtner, D. F. Phillips, D. Sasselov, A. Szentgyorgyi, and R. L. Walsworth, "A laser frequency comb that enables radial velocity measurements with a precision of 1 cm s^{-1}," Nature **452**(7187), 610–612 (2008).
34. T. Steinmetz, T. Wilken, C. Araujo-Hauck, R. Holzwarth, T. W. Hänsch, L. Pasquini, A. Manescau, S. D'Odorico, M. T. Murphy, T. Kentischer, W. Schmidt, and T. Udem, "Laser frequency combs for astronomical observations," Science **321**(5894), 1335–1337 (2008).
35. D. A. Braje, M. S. Kirchner, S. Osterman, T. Fortier, and S. A. Diddams, "Astronomical spectrograph calibration with broad-spectrum frequency combs," Eur. Phys. J. D **48**(1), 57–66 (2008).
36. G. Q. Chang, C.-H. Li, D. F. Phillips, R. L. Walsworth, and F. X. Kärtner, "Toward a broadband astro-comb: effects of nonlinear spectral broadening in optical fibers," Opt. Express **18**(12), 12736–12747 (2010).
37. T. Wilken, C. Lovis, A. Manescau, T. Steinmetz, L. Pasquini, G. Lo Curto, T. W. Hänsch, R. Holzwarth, and T. Udem, "High-precision calibration of spectrographs," Mon. Not. R. Astron. Soc. Lett. **405**(1), L16–L20 (2010).
38. C.-H. Li, A. G. Glenday, A. J. Benedick, G. Q. Chang, L.-J. Chen, C. Cramer, P. Fendel, G. Furesz, F. X. Kärtner, S. Korzennik, D. F. Phillips, D. Sasselov, A. Szentgyorgyi, and R. L. Walsworth, "*In-situ* determination of astro-comb calibrator lines to better than 10 cm^{-1}," Opt. Express **18**(12), 13239–13249 (2010).
39. F. Quinlan, G. Ycas, S. Osterman, and S. A. Diddams, "A 12.5 GHz-spaced optical frequency comb spanning >400 nm for near-infrared astronomical spectrograph calibration," Rev. Sci. Instrum. **81**(6), 063105 (2010).
40. A. J. Benedick, G. Q. Chang, J. R. Birge, L.-J. Chen, A. G. Glenday, C.-H. Li, D. F. Phillips, A. Szentgyorgyi, S. Korzennik, G. Furesz, R. L. Walsworth, and F. X. Kärtner, "Visible wavelength astro-comb," Opt. Express **18**(18), 19175–19184 (2010).
41. F. Bouchy, F. Pepe, and D. Queloz, "Fundamental photon noise limit to radial velocity measurements," Astron. Astrophys. **374**(2), 733–739 (2001).
42. C.-H. Li, G. Q. Chang, L.-J. Chen, D. Phillips, F. Kärtner, and R. Walsworth, "Lab demonstration and characterization of a green astro-comb," Advanced Solid-State Photonics (ASSP) (2011), paper AME5.

1. Introduction

Fiber-optic Cherenkov radiation (FOCR), also known as dispersive wave generation or non-solitonic radiation, describes the radiation from a fiber-optic soliton when perturbed by

#140545 - $15.00 USD Received 4 Jan 2011; revised 22 Feb 2011; accepted 10 Mar 2011; published 23 Mar 2011

higher-order fiber dispersion [1–5]. First theoretically studied in 1986, FOCR has attracted renewed research interest in company with the advent of photonic crystal fibers (PCFs) whose properties can be flexibly engineered [6]. For example, controlling a PCF's hole-size and inter-hole spacing results in two zero-dispersion wavelengths (ZDWs) which in turn give rise to two FOCR bands [7]. As a matter of fact, deliberate designs allow the presence of three ZDWs [8]; such a PCF would accommodate a variety of novel phenomena arising from phase-matched interactions between soliton and the resulting FOCR [9]. To date, most of FOCR research in PCFs is carried out in the context of suppercontinuum generation since FOCR extends the spectrum towards shorter wavelength [10–18]. Supercontinuum generation requires that the pump pulse propagate in the anomalous dispersion regime and form a higher-order soliton. To achieve a SC without substantial spectral gaps, the pump's center wavelength needs to be close to the fiber's ZDW so that the generated FOCR merges with the spectral components building up from other nonlinear effects. As this wavelength separation increases, FOCR manifests as an isolated spectrum that corresponds to a wavelength up-conversion or down-conversion of the pump depending on the sign of the third-order dispersion [7,19–22]. The up-conversion FOCR is of particular importance due to its capability of converting near-infrared (NIR) ultrafast lasers (e.g., Ti:Sapphire laser) to their counterparts in the visible wavelength range. The resulting ultrafast sources are desired in many applications, such as multi-photon microscopy, fluorescence spectroscopy, and optical coherence tomography. It is widely believed that FOCR generates resonant, narrowband (i.e., ~10 nm in the visible wavelength range) spectrum with relatively low conversion efficiency (~10%). These two drawbacks have hampered many real-world applications that demand high photon flux with a broadband coverage. Recently, we have explored the dependence of these two quantities (i.e., bandwidth and conversion efficiency) on the NIR pump-pulse's parameters (such as duration and pulse energy), and have demonstrated FOCR featuring high efficiency (>40%), broadband spectrum (>50 nm), and low threshold (<100 pJ for pulse energy) [23]. Such a dramatic improvement results from using few-cycle pump pulses to drive the radiation.

Generation of few-cycle laser pulses and their applications for investigating ultrafast processes in physics and chemistry have received a great deal of research attention [24]. While FOCR excited by few-cycle pulses has been pursued for different purposes (e.g., investigation of soliton-trapped FOCR [25] and synthesis of single-cycle pulses [26]), a thorough and detailed study of FOCR emphasizing bandwidth and conversion efficiency in this new regime is yet absent.

In this paper, we both theoretically and experimentally investigate FOCR in the few-cycle regime. In Ref. [23], we have identified three characteristic propagation scales: 1) initial buildup stage in which FOCR acquires most (>90%) of its energy; 2) quasi-independent propagation with minimal interaction with its host soliton; and 3) strong interaction with the host soliton that is decelerated by stimulated Raman scattering (SRS). Since the FOCR spectrum splitting and trapping that take place in the 3rd stage has been well studied, we rather focus on the first two stages.

2. Underlying physics in the initial buildup stage: phase-matching revisited by introducing *coherence length*

Propagation of an ultrashort pulse inside an optical fiber is well modeled by the generalized nonlinear Schrödinger (GNLS) equation [27]

$$\frac{\partial A}{\partial z}+\left(\sum_{n=2}^{\infty}\beta_n\frac{i^{n-1}}{n!}\frac{\partial^n}{\partial T^n}\right)A=i\gamma\left(1+\frac{i}{\omega_0}\frac{\partial}{\partial T}\right)\left(A(z,T)\int_{-\infty}^{+\infty}R(t')\left|A(z,T-t')\right|^2dt'\right), \quad (1)$$

#140545 - $15.00 USD Received 4 Jan 2011; revised 22 Feb 2011; accepted 10 Mar 2011; published 23 Mar 2011

where $A(z,t)$ represents the input pulse's amplitude envelope. $\beta_n = \dfrac{\partial^n \beta(\omega)}{\partial \omega^n}$ is evaluated at the central frequency ω_0 of the input pulse. γ is the nonlinear parameter of the fiber and $\beta(\omega)$ the fiber's dispersion curve. $R(t)$ describes both the instantaneous electronic and delayed molecular responses (i.e. SRS) of fused silica, and is defined as

$$R(t) = (1-f_R)\delta(t) + f_R[(f_a + f_c)h_a(t) + f_b h_b(t)]. \quad (2)$$

Typical values of f_R, f_a, f_b, and f_c are 0.245, 0.75, 0.21, and 0.04, respectively [28]. Isotropic Raman response $h_a(t)$ and anisotropic Raman response $h_b(t)$ are defined as $h_a(t) = \Theta(t)(\tau_1^2 + \tau_2^2)/(\tau_1 \tau_2^2)\exp(-t/\tau_2)\sin(t/\tau_1)$ and $h_b(t) = \Theta(t)(2\tau_b - t)/\tau_b^2 \exp(-t/\tau_b)$, where τ_1, τ_2, and τ_b have values of 12 fs, 32 fs, and 96 fs, respectively. $\Theta(t)$ is the Heaviside step function. If higher-order dispersion (i.e. $\beta_n, n>2$), self-steepening, and SRS are absent Eq. (1) under $\beta_2 < 0$ supports fundamental soliton solution with propagation constant $\beta_s(\omega) = \beta_0 + \beta_1(\omega - \omega_0) + (1-f_R)\gamma P_0/2$. The peak power P_0 and full-width-half-maximum (FWHM) duration T_0 are related by the soliton area theorem, i.e., $(1-f_R)\gamma P_0 = 3.1|\beta_2|/T_0^2$.

Optical soliton—a non-dispersive pulse with the propagation constant $\beta_s(\omega)$ —is a consequence of interplay between anomalous dispersion and self-phase modulation (SPM). Higher-order dispersion exerts perturbation onto a soliton and enforces it to shed away energy carried out by a dispersive pulse; the pulse travels with a propagation constant which coincides with the fiber's dispersion curve $\beta(\omega)$. Evidently, two sources contribute to the FOCR at position $z + \Delta z$: 1) the FOCR at z, which propagates Δz distance and acquires an extra phase due to fiber dispersion; and 2) the new radiation emitted by the soliton as it moves from z to $z + \Delta z$. Depending on their phase difference, these two fields add up constructively or destructively. If the phase-matching condition, i.e. $\beta(\omega) = \beta_s(\omega)$, is satisfied for any frequency, the two fields stay in-phase all the time and the generation of FOCR is maximized. In reality, however, the phase-matching condition only holds at a certain discrete frequencies. This is owing to the fact that $\beta_s(\omega)$ is a linear function of frequency (that is why soliton is non-dispersive) while $\beta(\omega)$ could be highly oscillatory for specially engineered dispersion. These phase-matched frequencies grow up monotonically along the propagation due to constructive interference. In contrast, non-phase-matched frequencies experience destructive interference and thus are strongly suppressed given enough propagation distance. Such a phase-sensitive mechanism explains why FOCR is widely regarded as a resonance process and forms a narrowband spectrum—a popular image one bears in mind. To describe phase-mismatch caused spectral narrowing, we introduce a new quantity L_c —*coherence length*— defined as $L_c(\omega) = \pi / |\beta(\omega) - \beta_s(\omega)|$. Plugging in the expression of the soliton's propagation constant, after a little math, the coherence length can be expressed as a function of fiber's dispersion and input soliton peak power,

$$L_c(\omega) = \frac{\pi}{|\beta(\omega) - \beta_s(\omega)|} = \frac{\pi}{\left|\sum_{n\geq 2} \frac{(\omega-\omega_0)^n}{n!}\beta_n(\omega_0) - \frac{(1-f_R)\gamma P_0}{2}\right|}. \quad (3)$$

Apparently L_c characterizes the fiber length where a π phase-slip accumulates between the CR radiated by a soliton located at $z + L_c$ and the radiation that emerges at z and then

#140545 - $15.00 USD Received 4 Jan 2011; revised 22 Feb 2011; accepted 10 Mar 2011; published 23 Mar 2011

propagates to $z + L_c$. A destructive interference between these two radiations diminishes the efficient power buildup of a FOCR.

It is noteworthy that the physical picture behind FOCR is quite universal in nonlinear optics, especially in illustrating $\chi^{(2)}$ -initiated nonlinear phenomena, such as second-harmonic generation, sum-frequency generation, difference-frequency generation, etc. For example, when driven by femtosecond pulses, optical rectification—a degenerate difference-frequency generation—gives rise to generation of broadband spectrum located at terahertz regime. In fact, we have borrowed the concept of coherence length from the terahertz community. In the context of ultrafast terahertz generation, coherence length quantifies the matching between the terahertz pulse's phase-velocity and the optical pulse's group velocity [29]. This velocity-matching is intrinsically equivalent to phase-matching required for efficient three-wave (i.e. terahertz frequency and two optical frequencies for optical rectification) mixing in a $\chi^{(2)}$ nonlinear process.

For a $\chi^{(2)}$ nonlinear process, it is the thickness of the nonlinear crystal that largely determines phase-matching bandwidth. Thus a thinner crystal is desired to achieve broader bandwidth at the cost of a decrease in conversion efficiency. Since FOCR shares a similar physical mechanism, one may ask whether such a tradeoff between bandwidth and conversion efficiency also exists for FOCR. Answering this question necessitates numerically solving the GNLS equation.

3. Continuum generation in the few-cycle regime

To investigate the effect of coherence length, we perform simulations for a fundamental soliton propagating in a PCF. The mode-field diameter of the PCF is 1.2 μm. The group-velocity dispersion shown in Fig. 1(a) indicates that the PCF has a ZDW at 0.71 μm. Also plotted in the same figure are the coherence lengths for three fundamental solitons with different FWHM duration (i.e. T_0) or center wavelength (i.e. λ_0) which are specified in the legend of Fig. 1(a). These three curves share similar features:

(1) The coherence length goes to infinity at the phase-matching wavelength which is shorter than the soliton center wavelength due to a positive third-order dispersion (i.e. $\beta_3(\omega_0) > 0$).

(2) Similar to a $\chi^{(2)}$ nonlinear process, the FOCR phase-matching bandwidth depends on propagation distance. At the vicinity of the phase-matching wavelength, which is practically useful, the phase-matching bandwidth decreases with the increase of propagation distance.

(3) Below a certain distance L_{con} (we refer to it as continuum length hereafter; see the label in Fig. 1(a) as an example), phase mis-match $< \pi$ is achieved for a continuous, broad wavelength range covering hundreds of nanometers. For shorter soliton duration (equivalent to increasing soliton peak power) or increasing soliton center wavelength blue-shifts the phase-matching wavelength while the continuum length decreases accordingly.

The broad phase-matching bandwidth around the continuum length strongly suggests that a continuum might build up spanning between the phase-matching wavelength and the soliton center wavelength. To verify such a prediction, we take each of the three fundamental solitons as the input and numerically solve the GNLS equation. Figures 1(b)–1(d) record the resulting spectral evolution for these three solitons propagating up to 10 cm; the spectra normalized to their peak power at each position are shown in logarithm scale. Despite calculated for different inputs, the corresponding spectra evolve following a similar pattern:

#140545 - $15.00 USD Received 4 Jan 2011; revised 22 Feb 2011; accepted 10 Mar 2011; published 23 Mar 2011

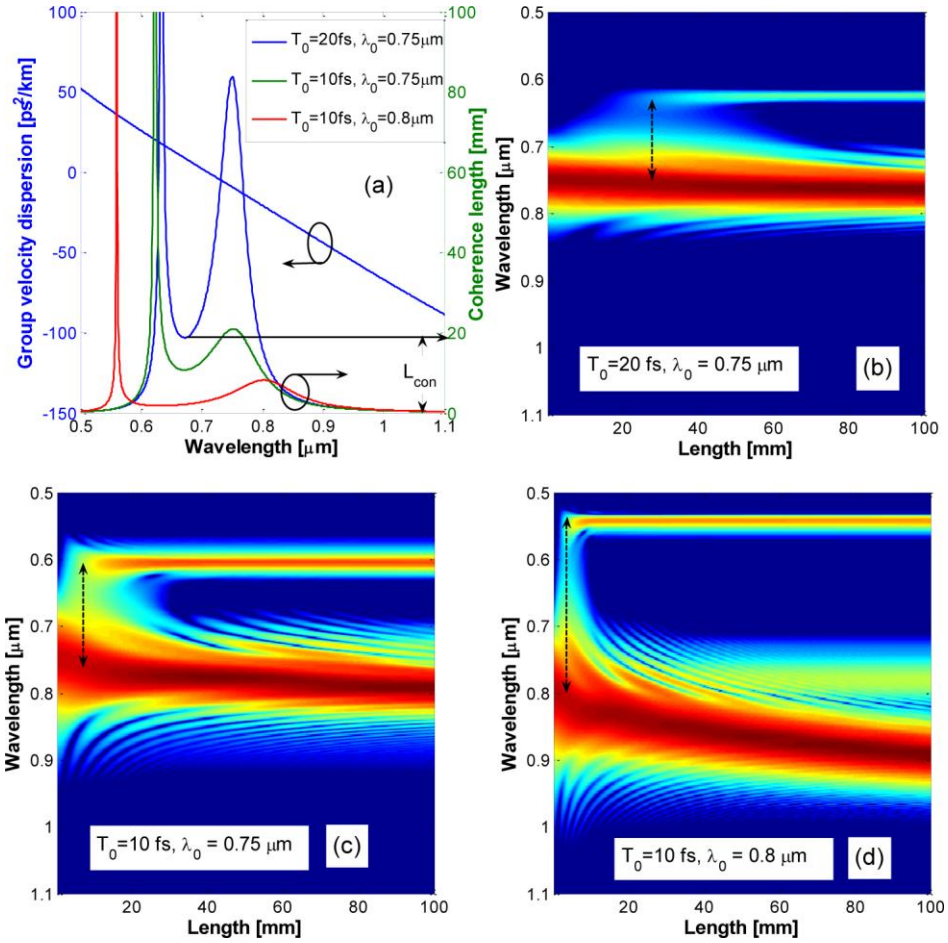

Fig. 1. (a) the PCF's group velocity dispersion and calculated coherent length for three fundamental solitons with different peak power or center wavelength (see the legend). L_{con} labels the continuum length for the blue curve; (b)-(d) spectrum evolution along propagation distance for fundamental solitons with different FWHM duration or different center wavelength (as indicated in each figure). The spectrum intensity is shown in logarithm scale. The double-arrow line marks the continuum that connects the phase-matching wavelength and the soliton center wavelength.

(1) As the soliton enters the PCF, higher-order dispersion together with other nonlinear effects (e.g., self-steepening and SRS) initiates the FOCR, which primarily extends to the shorter wavelength as predicted by the coherence length shown in Fig. 1(a).

(2) The blue edge of the radiation eventually reaches the phase-matching wavelength. Meanwhile, a continuum (marked by the double-arrow line in each figure), spanning between the soliton's center wavelength and the phase-matching wavelength, forms at the distance close to the calculated continuum length L_{con}.

(3) At the distance of about $2L_{con}$, the continuum nearly vanishes and an isolated spectrum builds up which stays almost unchanged for further propagation.

(4) The phase-matching wavelength (i.e. the FOCR peak wavelength) obtained by numerically solving the GNLS equation is always shorter than predicted by Eq. (3). This discrepancy arises from the spectral recoil effect: to preserve the entire-

#140545 - $15.00 USD Received 4 Jan 2011; revised 22 Feb 2011; accepted 10 Mar 2011; published 23 Mar 2011

spectrum's center-of-mass, the emitted FOCR red-shifts the soliton spectrum, which in turn emits new FOCR at even shorter wavelength [14]. Consequently, the resulting FOCR is further blue-shifted with a broader bandwidth compared to the prediction from Eq. (3).

Generation of continuum highly depends on input soliton's duration. A comparison between Fig. 1(b) and Fig. 1(c) reveals that using a shorter, few-cycle pulse as the input favors continuum generation accompanied by higher power conversion efficiency and better spectral flatness. For most reported FOCR experiments, which exploit input pulses of ~100-fs duration, the continuum generation is extremely weak and thus not observed.

4. Higher conversion efficiency in the few-cycle pulse regime

Results in Fig. 1 confirm the physical picture described in section 2; that is, FOCR at a propagation distance $z+\Delta z$ includes two parts: the radiation accumulated before z and new radiation as the soliton travels from z to $z+\Delta z$. Note that the new added radiation $\Delta E_{CR}(\omega)$ is proportional to Δz as well as to the soliton's spectral amplitude at ω. Therefore, a soliton with shorter duration extends more in the spectral domain which enhances FOCR generation, leading to a higher conversion efficiency as indicated by comparing Fig. 1(c) with Fig. 1(b).

The simulation performed in last section has assumed fundamental solitons as the input, which possess low pulse energy. For example, the soliton centered at 0.75 μm with 20-fs duration (i.e. the simulation input for generating Fig. 1(b)) is of only 12 pJ. The typical pulse energy in FOCR experiments is normally at ~1 nJ level. In this scenario, the input hyperbolic secant pulse becomes a *N*th-order soliton rather than a fundamental soliton; the soliton order *N* is given by

$$N=\sqrt{0.32(1-f_R)\gamma P_0 T_0^2/|\beta_2|}\propto\sqrt{E_0 T_0}, \tag{4}$$

where E_0 is the soliton's energy. When perturbed by higher-order dispersion and SRS, a *N*th-order soliton becomes unstable and breaks into *N* fundamental solitons with different peak powers and durations [30]. The resulting *j*th ($1\le j\le N$) fundamental soliton has the peak power, duration, and energy given by $P_j=P_0(2N-2j+1)^2/N^2$, $T_j=T_0/(2N-2j+1)$, and $E_j=E_0(2N-2j+1)/N^2$, respectively. While all these fundamental solitons participate in the FOCR, their contributions differ dramatically. The first (corresponding to $j=1$) fundamental soliton, which possesses the shortest duration and highest peak power, has the strongest spectral amplitude at a given frequency and thus dominates the FOCR yield [31]. The coherence length may be extended to the following expression which is also valid for higher-order soliton as an input:

$$L_c(\omega)=\frac{\pi}{\left|\sum_{n\ge 2}\frac{(\omega-\omega_0)^n}{n!}\beta_n(\omega_0)-\frac{(2N-1)^2(1-f_R)\gamma P_0}{2N^2}\right|}. \tag{5}$$

Equation (4) indicates that, if soliton energy E_0 is fixed, soliton number *N* decreases with a reduction of soliton duration T_0. A less *N* results in a larger P_j, a shorter T_j, and a larger E_j, which in turn lead to a stronger FOCR carrying more shed energy. In other words, using a shorter soliton as the excitation pulse improves FOCR conversion efficiency.

#140545 - $15.00 USD Received 4 Jan 2011; revised 22 Feb 2011; accepted 10 Mar 2011; published 23 Mar 2011

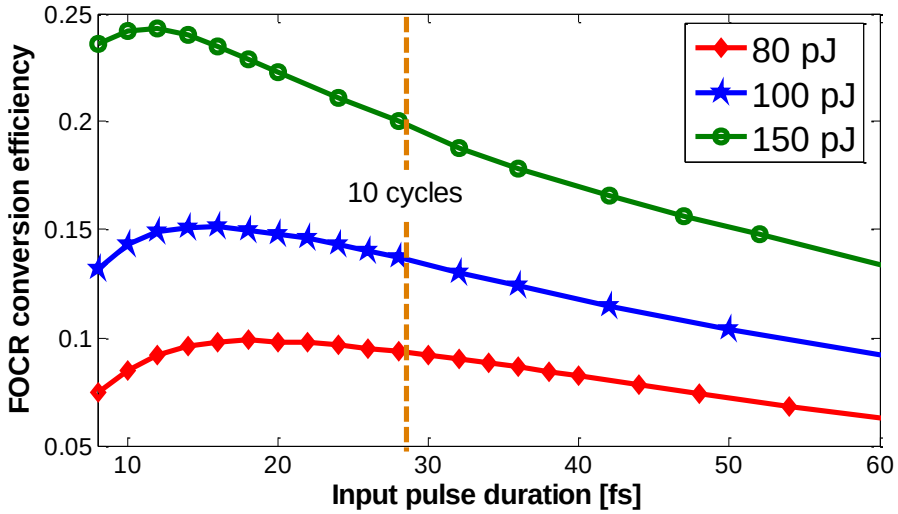

Fig. 2. Dependency of FOCR conversion efficiency on input pulse duration for different pulse energy. An optimum duration in maximizing conversion efficiency exists for a given input pulse energy; the optimum duration becomes shorter with increasing pulse energy. The orange dashed line indicates the duration that corresponds to a pulse of 10 cycles centered at 0.8 μm.

From above analysis, one might speculate that, with input pulse energy fixed, conversion efficiency may monotonically increase as the input pulse duration decreases. As a matter of fact, this is not true. It has been well known that, if T_0 is so small that the resulting soliton number is much less than 1, fiber dispersion overtakes the nonlinearity and no soliton can form. As a result, FOCR is absent. Therefore there must be an optimum pulse duration that maximizes conversion efficiency for a given input energy. Figure 2 plots dependency of FOCR conversion efficiency on input pulse duration for different pulse energy. Evidently, an optimum duration in maximizing conversion efficiency exists for a given input pulse energy, and it becomes shorter with increasing pulse energy. More specifically, the optimum duration decreases from 18 fs to 12 fs as the input pulse duration increases from 80 pJ (red line with diamond marker) to 150 pJ (green line with square marker); the conversion efficiency at the optimum duration goes up from 10% to 24%. For a given duration, increasing input pulse energy always improves conversion efficiency. The dashed, orange line marks the duration corresponding to 10 carrier oscillation cycles at 0.8 μm. The fact that the optimum duration is less than 10 optical cycles even for a moderate energy level (80 pJ - 150 pJ) indicates that FOCR in the few-cycle regime is highly desirable to achieve higher conversion efficiency and stronger FOCR pulse. The soliton order ranges 1.5 – 2 at the optimum duration.

5. Broader bandwidth in the few-cycle regime

In the physical picture that qualitatively describes FOCR generation and evolution, the emitted FOCR linearly propagates inside the fiber, only experiencing fiber dispersion. Such a model is valid when the conversion efficiency is low so that the resulting weak FOCR pulse creates negligible nonlinear effects. Apparently this is not the case for FOCR in the few-cycle regime featuring high conversion efficiency. In this new regime, FOCR pulse may carry ~40% of the total input energy [23], strong enough to cause nonlinear effects (e.g., SPM) which in turn reshape the FOCR pulse and broaden its optical spectrum.

#140545 - $15.00 USD Received 4 Jan 2011; revised 22 Feb 2011; accepted 10 Mar 2011; published 23 Mar 2011

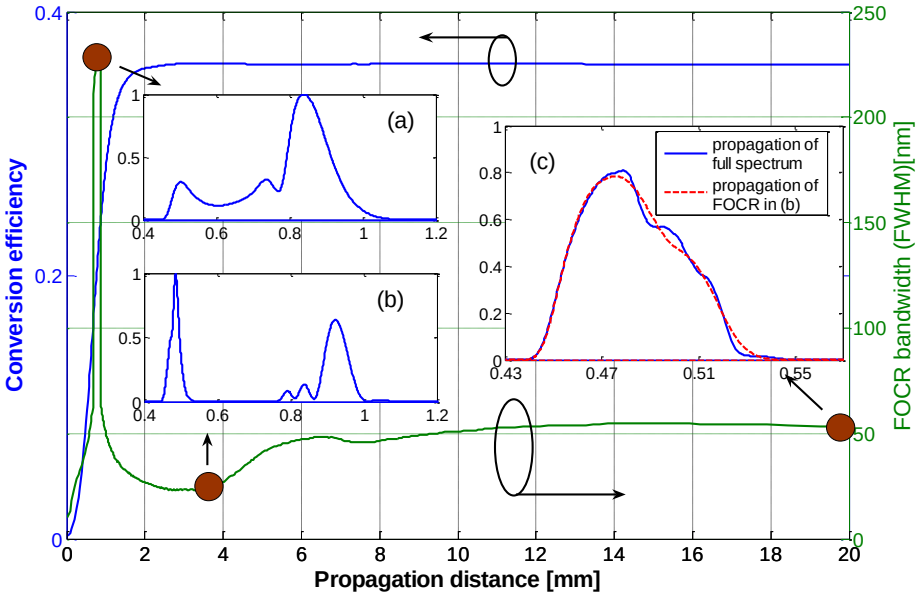

Fig. 3. Evolution of FOCR conversion efficiency and spectral bandwidth along propagation distance for a 10-fs hyperbolic secant pulse centered at 0.8 μm with 300-pJ pulse energy. Insets (a) and (b) plot spectra corresponding to the maximum and minimum bandwidth. Further propagation of spectrum recorded in (b) up to 2 cm results in the FOCR spectrum shown as the blue, solid line in inset (c). If we propagate only the FOCR spectrum (i.e., spectrum in 0.4-0.6 μm), the corresponding spectrum at 2-cm distance is denoted by the red, dashed curve. See the text for details. Note that the spectra are shown in linear scale.

Figure 3 plots the evolution of FOCR conversion efficiency and spectral bandwidth along propagation distance for an input 10-fs pulse of hyperbolic secant shape centered at 0.8 μm with 300-pJ pulse energy. The spectral bandwidth is FWHM of the optical spectrum located in the range of 0.4-0.7 μm. The spectra at 0.8 mm, 4 mm and 20 mm are presented as inset (a)-(c), respectively. A comparison of FOCR spectral bandwidth reveals a three-stage evolution, which normally does not coincide with the aforementioned three-stage process in terms of conversion efficiency:

(1) 0-0.8 mm: rapid growing of spectral bandwidth due to continuum generation as a result of large phase-matching bandwidh. At the end of this stage, the FOCR continuum partially overlaps with the red-shifted soliton spectrum, forming a smooth supercontinuum (spectrum in inset (a) of Fig. 3) which spans more than one octave. The spectrum between 0.4 and 0.7 μm accounts for ~20% of the total input energy.

(2) 0.8-4 mm: fast narrowing of the spectrum within 0.4-0.7 μm due to the reduced phase-matching bandwidth as propagation proceeds beyond the coherence length. The continuum's short-wavelength edge concentrates more and more energy, while the longer-wavelength side diminishes during propagation, leading to the formation of an isolated FOCR spectrum. This stage ends up with a FOCR spectrum of 23 nm bandwidth, which carries 35% of the total input energy. As the spectrum in inset (b) of Fig. 3 shows, the narrowband FOCR spectrum and its host pumping spectrum are well separated with a spectral gap of ~300 nm.

(3) 4-20 mm: gradual broadening of the isolated FOCR spectrum up to 53 nm. The constant conversion efficiency in this stage indicates that there is no further energy exchange between the isolated FOCR spectrum and the residual pump. In the time

#140545 - $15.00 USD Received 4 Jan 2011; revised 22 Feb 2011; accepted 10 Mar 2011; published 23 Mar 2011

domain, the residual pump pulse travels faster than the FOCR pulse. Their temporal separation increases during propagation and thus the nonlinear interaction between them diminishes continuously. To verify that the FOCR pulse propagates almost independently from the residual pump pulse in this stage, we seed the GNLS equation with the FOCR spectrum at 4-mm distance (i.e. the isolated spectrum within 0.4-0.6 μm in inset (b) of Fig. 3), and propagate it for 16 mm; the resulting spectrum is plotted in inset (c) as the red, dashed curve. Clearly, the two spectra perfectly overlap on the short wavelength side (0.43-0.47 μm) and deviate slightly on the long wavelength side (0.47-0.55 μm) while they possess the same energy (i.e., integrated area under both curves). The deviation arises from cross-phase modulation (XPM) exerted by the residual pump pulse whose trailing tail overlaps with the FOCR pulse's leading tail. Propagating in the normal dispersion region, the FOCR pulse develops positive chirp; that is, its leading tail corresponds to the longer wavelength. That explains why such XPM only modifies the FOCR's long wavelength side, leaving the other side unaffected. The results shown in inset (c) also indicate that main mechanism for the FOCR spectral broadening from 23 nm to 53 nm is attributed to the nonlinear effects (e.g., SPM and self-steepening) caused by the FOCR pulse itself. Apparently, a higher FOCR conversion efficiency—a consequence when pumped in the few-cycle regime—results in a stronger FOCR pulse which facilitates the broadening process.

Note that the concept of coherence length explains the buildup of the FOCR in the first two stages. In the third stage in which CR emission stops, coherence length is not meaningful since interaction between CR and the pump pulse is absent. As for further propagation beyond 20 mm, part of the residual pump develops into a soliton (hereafter, we refer it as Raman soliton) which continuously shifts towards longer wavelength driven by SRS, and as a result, slows down. Eventually the FOCR pulse catches up with the decelerating Raman soliton; their strong nonlinear interaction splits the FOCR spectrum into two well-separated parts. The shorter wavelength part will be captured by the Raman soliton. Detailed studies on FOCR spectral splitting and trapping have been presented in Refs. [23] and [25].

6. Experimental results

Using a home-built 85-MHz Ti:Sapphire laser emitting ~10-fs pulses to pump a commercially available PCF, we have experimentally investigated FOCR in the few-cycle regime. The PCF has a ZDW at 710 nm with a dispersion curve shown in Fig. 1(a). A detailed description of the whole setup can be found in Ref. [23].

Figure 4(a) records the FOCR spectra generated by three PCFs with different lengths: 2 mm, 4 mm, and 2 cm; the input pulse energy coupled into these fibers is fixed at 300 pJ. While the coupled spectrum [inset in Fig. 4(a)] is not of hyperbolic shape, the experimental results well reproduce the main features of the three-stage evolution discussed in session 5 and depicted in Fig. 3:

(1) As expected for the case of a 2-mm PCF, a broadband continuum develops at the pump's short wavelength side—a signature for the first stage.

(2) At the output of the 4-mm PCF, a narrowband (20-nm FWHM), isolated FOCR spectrum builds up; the resulting spectral recoil pushes the residual pump spectrum toward longer wavelength [see Fig. 1(d)]. The experimental FOCR spectrum is close to the theoretical prediction [inset (b) in Fig. 3] in terms of FWHM bandwidth (20 nm vs. 23 nm) and spectral shape.

(3) Emanating from the 2-cm PCF, the narrowband FOCR spectrum broadens to 50 nm due to its nonlinear propagation. SRS continuously red-shifts the residual pump spectrum, from which a Raman soliton gradually emerges.

#140545 - $15.00 USD Received 4 Jan 2011; revised 22 Feb 2011; accepted 10 Mar 2011; published 23 Mar 2011

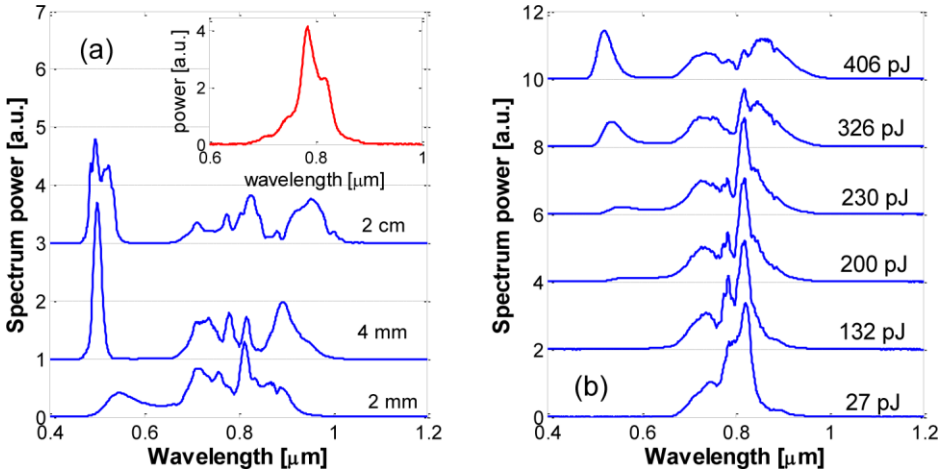

Fig. 4. (a) Evolution of FOCR spectrum with increased PCF length, labeled as 2 mm, 4 mm, and 2 cm, respectively. The input pulse energy is fixed at 300 pJ. Inset shows the laser spectrum coupled into the fiber (i.e., the optical spectrum at the beginning of the PCF). (b) Evolution of FOCR spectrum with increased input pulse energy for the 2-mm long PCF.

The dependence of continuum generation on input pulse energy is also explored using the 2-mm PCF. Figure 4(b) plots the resulting spectra as we vary input pulse energy. Similar to the spectral evolution with respect to increased PCF length, a continuum appears with the input pulse energy increased; further increase results in an isolated FOCR spectrum growing up at the continuum's short wavelength side. Such an evolution trend also indicates that the continuum length becomes shorter with increased input pulse energy.

As the results in Fig. 2 show, using few-cycle pulses to excite FOCR enhances its conversion efficiency, leading to a stronger FOCR pulse; the corresponding stronger nonlinearity eventually leads to a broader FOCR spectrum in the visible wavelength range. In other words, FOCR excited by few-cycle pulses allows achieving broadband visible-wavelength spectra from relatively low-energy ultrafast sources. For example, scaling up the repetition rate of a Ti:sapphire femtosecond oscillator beyond 1 GHz is inevitably accompanied by low pulse energy (<1 nJ). Such high repetition-rate sources are desired in many applications, such as frequency metrology, optical arbitrary waveform generation, and high speed A/D conversion, to name a few. To demonstrate that FOCR in the few-cycle regime constitutes a powerful wavelength up-conversion tool to efficiently convert a NIR, GHz laser source into its broadband counterpart in the visible wavelength range, we switch to a home-built, 1 GHz Ti:sapphire oscillator as the pump source, centered at 0.83 μm with ~140 nm bandwidth and ~800 mW average power. Figure 5 presents the FOCR spectra generated by 10-cm PCFs with different ZDW, i.e., 710 nm, 735 nm, and 750 nm. The maximum powers coupled into these fibers are 210 mW, 250 mW, and 190 mW, respectively [see the figure legend that specifies each fiber's ZDW and coupled power]. The relatively low coupling efficiencies into these PCFs are due to chromatic dispersion caused by the singlet coupling lenses. Higher coupled powers are expected if achromatic coupling lenses are employed. The FOCR spectrum, its center wavelength mainly determined by the phase-matching condition, shifts toward longer wavelength along with increasing the PCF's ZDW. Indeed, 10-cm length of PCF is enough to substantially slow down the Raman soliton (emerging from the residual pump) so that it has a considerable overlap with the FOCR pulse; the overlap-introduced XPM manifests as amplitude modulation onto the FOCR spectra shown in Fig. 5. With 20-30% conversion efficiency, the resulting FOCR spectra, locating in the visible wavelength range, exhibit a bandwidth of 50-70 nm.

#140545 - $15.00 USD Received 4 Jan 2011; revised 22 Feb 2011; accepted 10 Mar 2011; published 23 Mar 2011

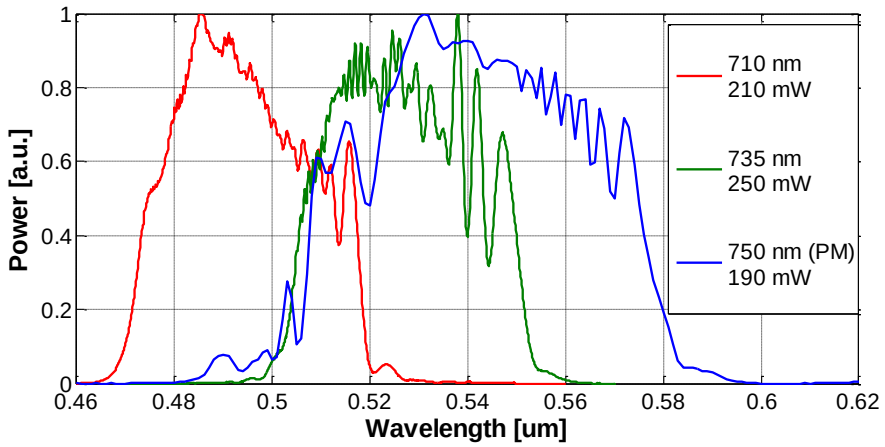

Fig. 5. FOCR spectra generated by 10-cm PCFs with different ZDWs, i.e., 710 nm (red curve), 735 nm (green curve), and 750 nm (blue curve). The one with 750-nm ZDW is a polarization maintaining (PM) PCF.

Recent years have seen growing research interest in optimizing femtosecond-laser based frequency combs for astrophysical spectrograph calibration ("astro-combs") [32–40]. Through precision radial velocity (PRV) observation, astro-combs hold the promise to enable the search for Earth-like extra-solar planets (exoplanets), direct observation of cosmological deceleration, and the study of temporal variation of fundamental constants. Astro-combs in the visible wavelength range are of particular importance because, in this wavelength region (400-600 nm), emission from Sun-like stars provides the largest photon flux as well as high-quality spectral features most suited for PRV observation [41]. While astro-combs in the blue and green have been demonstrated via second harmonic generation of NIR source combs, they exhibit narrow bandwidth (2 nm for the green astro-comb [37] and 15 nm for the blue [40]). In this scenario, the broadband, highly efficient, GHz FOCR in the few-cycle pulse regime emerges as a powerful wavelength up-conversion tool to implement a broadband astro-comb in the visible wavelength range. As a proof-of-concept, we have demonstrated a broadband green astro-comb using this method [42].

7. Discussion and conclusion

In this paper, we have both theoretically and experimentally studied FOCR in the few-cycle regime, with a focus on its evolution before spectral splitting due to the decelerated Raman soliton. Although FOCR originates from $\chi^{(3)}$ nonlinear susceptibility of an optical fiber, its buildup and initial evolution resembles well-known $\chi^{(2)}$ nonlinear effects, such as second-harmonic generation, sum-frequency generation, difference-frequency generation, and optical rectification. A universal feature of these phenomena is that they all require phase-matching to achieve efficient power conversion. At the initial evolution stage of FOCR, its bandwidth is determined by phase-matching condition in a manner similar to $\chi^{(2)}$ nonlinear process; that is longer propagation leads to narrower bandwidth. Inspired by such a resemblance, we have introduced the coherence length for continuum generation—a characteristic phenomenon only evident for FOCR in the few-cycle regime. Coherence length also elucidates the physical mechanism behind the formation of an isolated FOCR spectrum that builds up at the short wavelength side of the continuum and experiences spectral narrowing. Inside a $\chi^{(2)}$ medium, normally the effect of $\chi^{(3)}$ is negligible and spectral broadening due to SPM is absent. Therefore spectral bandwidth is nearly exclusively determined by the phase-matching condition. In contrast, after the spectral narrowing due to limited phase-matching bandwidth,

#140545 - $15.00 USD Received 4 Jan 2011; revised 22 Feb 2011; accepted 10 Mar 2011; published 23 Mar 2011

FOCR is broadened as a consequence of nonlinear propagation. Such a nonlinear spectral broadening process is enabled by the high conversion efficiency achieved by exciting FOCR with few-cycle pulses.

In summary, we have demonstrated (both theoretically and experimentally) that FOCR in the few-cycle regime exhibits three unique features that are absent when pumped with often-used, long pulses: (1) continuum generation (may span one octave in connection with the pump spectrum), (2) high conversion efficiency (up to 40%), and (3) isolated FOCR spectra with broadband (70 nm experimentally obtained) coverage. Dependence of coherence length on fiber dispersion [see Eq. (3)] suggests that these three features can be engineered by tailoring the fiber's dispersion—a manufacturing flexibility readily provided by PCFs. For example, during the nonlinear propagation in which FOCR acquires more bandwidth, large normal dispersion quickly stretches the FOCR pulse up to hundreds of fs within a couple of centimeters, which dramatically reduces its peak power, weakens the nonlinear effects (e.g. SPM), and thus diminish the spectral broadening. Apparently, such a pulse-stretching effect can be suppressed by reducing the amount of normal dispersion in the FOCR spectral region. Consequently, the strengthened nonlinear effects will enhance the spectral broadening process. Furthermore, a reduced normal dispersion increases the coherence length, implying that constructive addition between the existing FOCR and newly emitted radiation takes place within a longer propagation distance. As a result, more input energy transfers to the FOCR, giving rise to an even higher conversion efficiency, which in turn benefits FOCR's spectral broadening.

Acknowledgments

This work was supported under National Aeronautics and Space Administration (NASA) grants NNX10AE68G, NNX09AC92G and National Science Foundation (NSF) grants AST-0905592 and AST-1006507.

#140545 - $15.00 USD Received 4 Jan 2011; revised 22 Feb 2011; accepted 10 Mar 2011; published 23 Mar 2011